



The origin of high hydrocarbon groundwater in shallow aquifer: experimental evidences from water-rock interaction

Shan Liu^{1,2} · Shihua Qi^{1,3} · Zhaohui Luo^{1,3} · Harold Wilson T. Mapoma⁴ · Zhihua Chen^{1,3} · Shenggao Cheng^{1,3}

Received: 15 May 2019 / Accepted: 23 September 2019 / Published online: 19 October 2019
© Springer-Verlag GmbH Germany, part of Springer Nature 2019

Abstract

The current studies had already revealed the hydrocarbons could migrate from relatively high hydrocarbon potential stratum to shallow groundwater by corrosion emission and extraction emission in karst area and further impact on human health. Then, the comprehensive experiments were used to understand the mechanism and process of hydrocarbon emission as a continuation of a long-term study on original high hydrocarbon groundwater in shallow Triassic aquifer, taking northwest Guizhou, China, as a reference. The results determined water-rock interaction that lead to the hydrocarbon emission into groundwater with salinity acting as the main driving force. Relatively high salinity promotes the rock corrosion and hydrocarbon emission in the study area. The hydrocarbon emission process varied with different strata, as the results show that the hydrocarbon uniformly distributed in T₂g³ than that in T₁yn⁴. Furthermore, the stratum with uniformly distributed hydrocarbon would likely contain high hydrocarbon groundwater, as determined by the process of sedimentation. In addition, “corrosion rate estimation method” and “mineral constituent estimation method” were firstly employed to estimate the hydrocarbon concentration in groundwater to date. Compared with the hydrocarbon concentration of local groundwater samples (0 to 0.14 mg L⁻¹), the result of “mineral constituent estimation method” was analogous to measured value of groundwater samples in the area (0.05 to 0.50 mg L⁻¹), indicating the concentration of hydrocarbon could be estimated by mineral constitutions of groundwater, which was related to the concentration of Ca²⁺ and Mg²⁺. Based on the methods and theories in this study, the concentration of original hydrocarbon in shallow groundwater could be estimated and help to understand the mechanism of water-rock interaction in shallow aquifer and original high hydrocarbon groundwater strategic assessment.

Highlights

- Experimental evidences show that hydrocarbons migrate from rocks to shallow groundwater by water-rock interaction.
- Sudden and sharp change in hydrocarbon reservoir stratum was observed at a higher dissolution rate unlike in source stratum.
- High hydrocarbon groundwater estimation was calculated using a mathematical equation.
- The estimated hydrocarbon groundwater was analogous to petroleum hydrocarbon in shallow groundwater studied
- The hydrocarbon concentration was related to the concentration of Ca²⁺ and Mg²⁺ in shallow groundwater in karst area.

Responsible editor: Philippe Garrigues

Electronic supplementary material The online version of this article (<https://doi.org/10.1007/s11356-019-06578-w>) contains supplementary material, which is available to authorized users.

✉ Shihua Qi
shihuaqi@cug.edu.cn

¹ State Key Laboratory of Biogeology and Environmental Geology, China University of Geosciences, Wuhan 430074, China

² School of Environmental Science and Engineering, Hubei Polytechnic University, Huangshi 435003, China

³ School of Environmental Studies, China University of Geosciences, Wuhan 430074, China

⁴ Physics and Biochemical Sciences, University of Malawi, The Polytechnic, Blantyre 3, Malawi

Keywords Original high hydrocarbon groundwater · Water-rock-hydrocarbon interaction · Hydrocarbon emission process · High hydrocarbon groundwater estimation

Introduction

Water-rock-hydrocarbon interaction represents a kind of physicochemical and mechanical interaction among groundwater, rocks, and hydrocarbons. It changes the chemical constituents of groundwater and stratum, especially the concentration and species of hydrocarbons (Kassotis et al. 2018; Sadykova and Dul'tseva 2017; Kharaka et al. 1986; Kerimov et al. 2017). It is a complicated physiochemical process where all the minerals and formation water are both reactants and products. A dynamic equilibrium between dissolution and precipitation at special temperature and pressure is attained in this process (Huang et al. 2017; Bouchaou et al. 2017; Ryzhenko et al. 2015; Onojake et al. 2015; Lasaga 1984). This interaction is also the key factor for oil-gas reservoir spatial evolution and functions in the whole diagenetic process (Cai et al. 1997). The process is influenced by the characteristics of oil basin, tectonic movement, stratum structure, mineral constituents, and hydrodynamic condition (Phan et al. 2018; Wang et al. 2018). Additionally, it is also the determining factor for hydrocarbons' migration from rock to shallow groundwater (Liu et al. 2017). In our daily life, the most direct manifestation for water-rock-hydrocarbon interaction is high hydrocarbon groundwater. In China, water quality standards for groundwater exist in relation to hydrocarbon levels. The standards stipulate that when the concentration of hydrocarbons in groundwater exceeds the limitation of China quality standard for groundwater grade III (0.05 mg/L for second-level drinking water source), it will be designated as "original high hydrocarbon groundwater." Hydrocarbons would reduce the quality and function of groundwater (Ugochukwu and Ochonogor 2018; Anatolievich and Mikhailovich 2017; Adekunle et al. 2017). The full understanding of the formation mechanism for the original high hydrocarbon groundwater in shallow aquifers is very important in groundwater environmental protection and sustainable economic development plans and strategies.

Currently, there is a great deal of research focused on the water-rock-hydrocarbon, which have been achieved in three ways. Firstly, the studies on the "source" known as source rock. This represents a kind of rock in which oil or gas could be generated, stored, and released (Tissot et al. 1974). Nowadays, the abundance, species, maturity of organic matter, and kerogen are used in oil-gas reservoir or metal mineral deposit exploration (Chalmers and Bustin 2017; Yu et al. 2018; Collins 1974). Moreover, it is the source of original high hydrocarbon groundwater. The geochemical characteristics of organic matter could also influence the species, concentration, and distribution of original high hydrocarbon groundwater (Tissot and Welte 1984). Secondly, studies through the

"process" known as geochemical kinetics of water-rock-hydrocarbon interaction have been done. In this scenario, an equivalent model in the laboratory is used to simulate and figure out the mechanism of hydrocarbon emission (HCE) in deep underground (Ryzhenko et al. 2015; Jia et al. 2018; Sadykova and Dul'tseva 2017). However, most of the studies were used for resource exploration. The theory for water-rock-hydrocarbon interaction in shallow aquifer remains to be fully understood. The third way is studies on "representations" known as original high hydrocarbon groundwater. Nowadays, original high hydrocarbon groundwater is usually used in oil-gas reservoir detection, diagenetic characteristic, and source analysis (Belousova et al. 1998; Yasaman et al. 2016; Huang et al. 2016). Otherwise, original high hydrocarbon groundwater would also lead to environmental problems (Liu et al. 2017). Petroleum hydrocarbon is the main contaminant in original high hydrocarbon groundwater. It is a complex compound that is composed of alkanes, cyclanes, and aromatics, which can potentially cause cancer, deformities, and mutations in humans (Bonzani et al. 2016; Logeshwaran et al. 2018; Poi et al. 2018). Moreover, original high hydrocarbon groundwater in shallow aquifer relates to people's daily life; it can easily influence the human health. Therefore, further studies about the emission process of original high hydrocarbon groundwater in shallow aquifer are in demand.

To fill the knowledge gap discussed above, a long-term research on original high hydrocarbon groundwater in the shallow Triassic aquifer of northwest Guizhou, China, was carried out since 2011. The study had already observed that there is strong water-rock interaction in the area. In this area, the Yongningzhen formation (T_{1yn}^4) and Guanling formation (T_2g^3) have relatively high hydrocarbon potential (Fig. S1). Based on the biomarker characteristics, hydrocarbons in stratum and groundwater had the same original source (Fig. S2), indicating the hydrocarbons migrated from rock to shallow groundwater by corrosion emission and extraction emission (Fig. 1). However, the migration process of hydrocarbons from rock to shallow groundwater still needs to be fully understood.

The present research is the continuation of the work that started in 2011 mentioned in the preceding paragraph. Different from the previous research studies, which designed an experimental model in the laboratory to figure out the mechanism of HCE in deep underground with high-temperature and high-pressure conditions (Ryzhenko et al. 2015; Jia et al. 2018; Cai et al. 1997), experiments in both field and laboratory were designed to figure out the HCE process in the study area with room temperature, pressure, and oxidation conditions. The results revealed that the HCE was controlled by the degree of water-rock interaction.

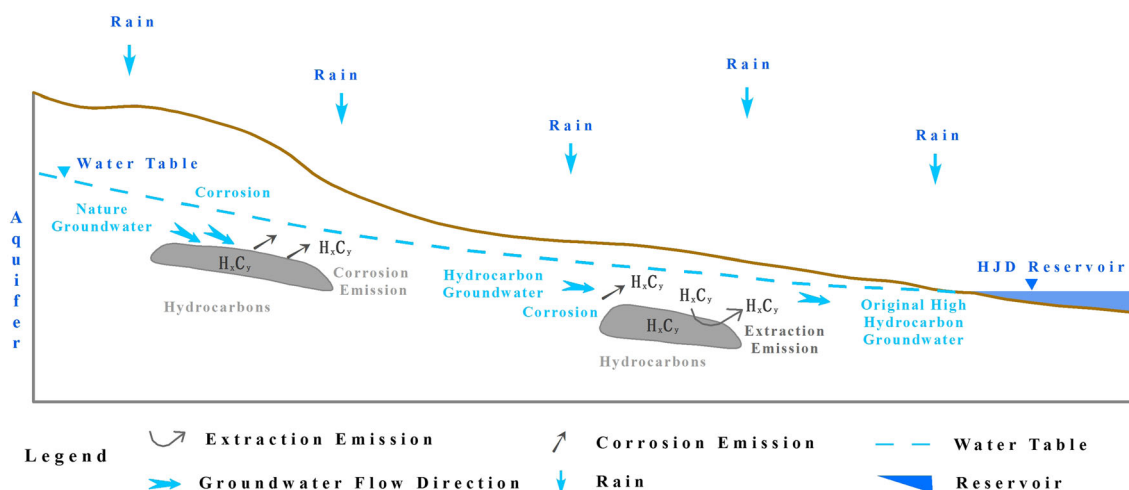


Fig. 1 The conceptual model of water-rock-hydrocarbon interaction in the study area

Additionally, salinity would promote high water-rock-hydrocarbon interaction and hydrocarbon release in the area. Moreover, the HCE process of T_{1yn}^4 and T_{2g}^3 shows a sudden changing and gradual changing, respectively. This indicated that hydrocarbons distributed uniformly in T_{2g}^3 . It revealed that the T_{2g}^3 would be the hydrocarbon source stratum in the area. Based on the reasonably assumed conditions, results of experiments in the laboratory and field, estimation equation of HCE was presented. Moreover, “corrosion rate estimation method” and “mineral constituent estimation method” were first time presented to estimate the hydrocarbon concentration in groundwater to date. Compared with the hydrocarbon concentration of local groundwater samples (0 to 0.14 mg L^{-1}), the result of “mineral constituent estimation method” was analogous to measured value of groundwater samples in the area (0.05 to 0.50 mg L^{-1}), indicating the concentration of petroleum hydrocarbon could be estimated by mineral constitutions of groundwater, which was related to the concentration of Ca^{2+} and Mg^{2+} . The HCE estimation equation and mineral constituent estimation method were reasonable in original high hydrocarbon groundwater in shallow aquifer strategic assessment. In practice, these outcomes indicated the concentration of original hydrocarbon in shallow groundwater could be estimated. More works could be pushed forward to help in understanding the mechanism of water-rock interaction in shallow aquifer and original high hydrocarbon groundwater strategic assessment.

Study area

Local social status

The study area is located in a rural area in northwest Guizhou, China (Fig. 2). It is a typical karst peak-cluster depression. Moreover, this area is one of the most backward economy

areas of Guizhou, as there are no heavy industries and organic industries developed here. The population is less than twenty thousand. In addition, most of them are aging people, who live with farming. From 2006 to 2016, there was no change in the way of land use (Fig. S3). With increased population, the woodland became smaller in this area. The arable land also decreased with the using of new farming technique and methods. Aerial maps showed well-developed karst and stony desertification covered most of the area. The land received less impact from human activities and remained in a nature state.

Hydrogeology and geology setting

The study area belongs to the Yangtze stratigraphic region. Emergence strata, in sedimentation progress, include Lower Triassic Yongningzhen (T_{1yn}), Middle Triassic Guanling (T_{2g}), and Middle Triassic Falang (T_{2f}) formations. The T_{1yn} formation is divided into middle-upper group (T_{1yn}^3) limestone (about 130 m thick) and upper group (T_{1yn}^4) breccia calcite-dolomite (about 89.5 m thick). The T_{2g} can be divided into lower group (T_{2g}^1) variegated mudstone (about 146 m thick), middle group (T_{2g}^2) massive limestone (about 263 m thick), and upper group (T_{2g}^3) collapse breccia calcite-dolomite with fissures (about 257 m thick). On the other hand, the T_{2f} has the characteristics of abundant limestone and dolomite interbedding with gypsum in a thickness of 46 m. Furthermore, several structures were found in the northeast region of this area (Fig. 2).

Rainfall controls recharge, while Hongjiadu (HJD) reservoir is the ultimate discharge base level, controlling runoff and the discharge. In the Dalongjing (DLJ) system, groundwater is recharged by rainfall. The surface water infiltrates into the groundwater system through caverns and fissures. The groundwater, which is controlled by the terrain and ultimate discharge base level, flows towards the northeast and discharges at the HJD reservoir (Fig. 2).

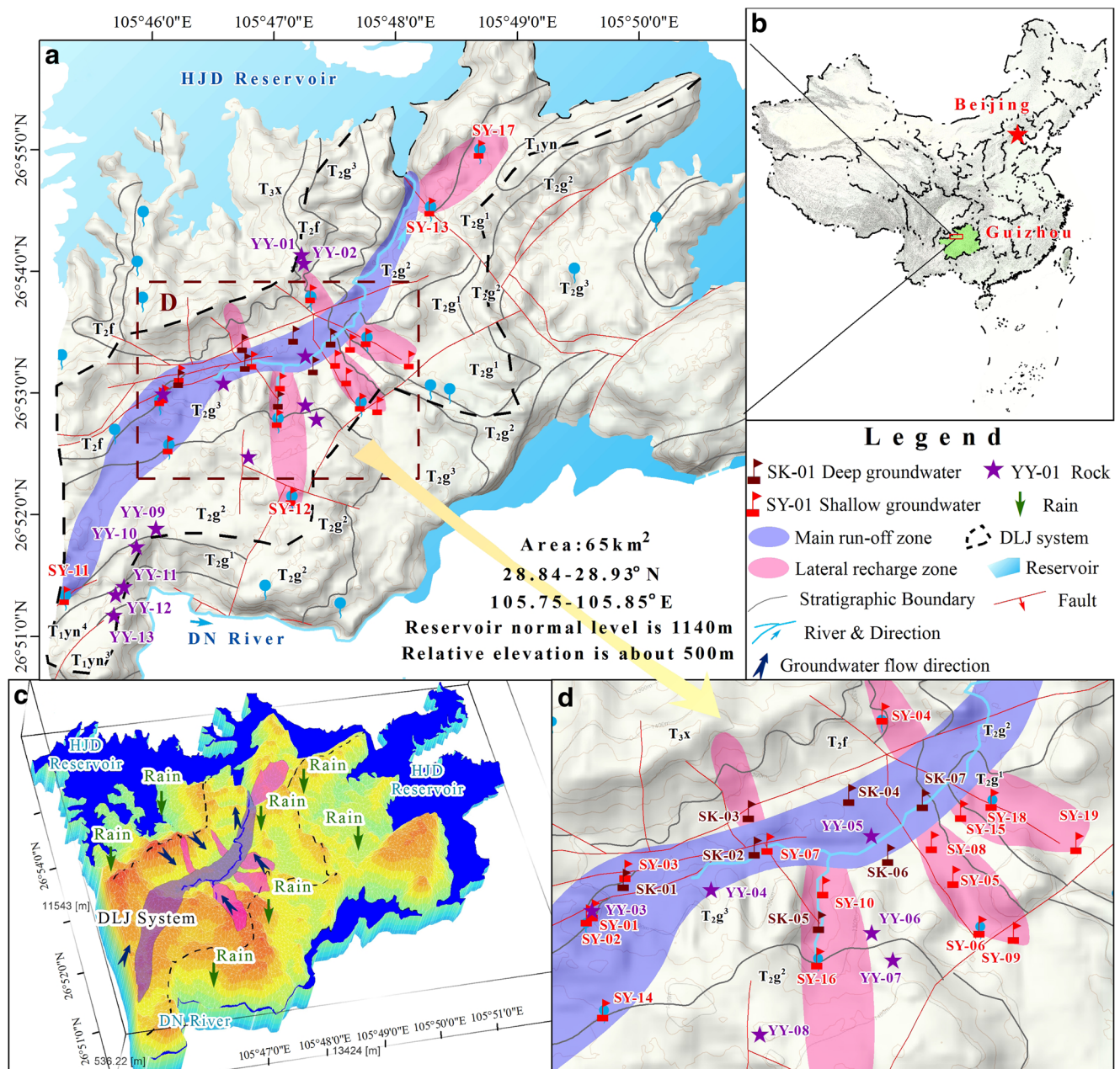


Fig. 2 General geological map showing location, hydrogeological condition, and sampling of the study area in the DLJ groundwater system, Guizhou. **A** shows hydrogeological condition and sampling. Shallow groundwater was collected at springs and shallow boreholes. Groundwater in shallow borehole collected at – 10 m below ground at

August 2015, while deep groundwater collected in deep borehole at – 100 m below ground at February 2016. All the corrosion experiment samples were buried 15 cm underground. **B** shows the location of the study area in Southwest China, Guizhou. **C** shows the hydrogeological condition with the 3D model. **D** shows the detail of sampling location

Materials and methods

Sampling

Based on the difference in hydrocarbon potential and lithology, thirteen rock samples were collected (Table S1). All rock samples were used for “corrosion experiment in the field.” Moreover, three of them were used for “corrosion emission

model,” while six of them were used for “dissolution emission model in the laboratory.” The pretreatment method of rock samples was different for different experiments. Additionally, based on the hydrogeological characteristics in the DLJ system, twenty-six groundwater samples, including ten spring samples, nine shallow borehole groundwater samples, and seven deep borehole groundwater samples, were collected (Fig. 2). All the results are shown in Tables S2–S4.

Experiments in the laboratory and field

Three experiments had been designed in this research to figure out the migration process of hydrocarbon from rock to groundwater and estimate the emission concentration of hydrocarbon to groundwater: (1) Corrosion experiment in the field: the experiment was mainly to figure out the corrosion rate for all strata in natural environment. (2) Corrosion emission model in the laboratory: it mainly focused on revealing the relationship between HCE and rock corrosion under ideal condition. The HCE rate and influencing factors of different strata were shown in this model. (3) Dissolution emission model in the laboratory: it was the accelerated model of “corrosion emission model in the laboratory.” In nature environments, hydrocarbon estimation is a long-term geological process. It always takes millions of years for hydrocarbons to migrate from rock to groundwater, indicating it is hard to observe the migrating process in a short period. Therefore, the migration process needs to be accelerated to figure out the estimation concentration of hydrocarbon. Moreover, the lithology of stratum in the area was carbonate rocks. Acid would dissolve the carbonate rocks within the short period. In that case, hydrochloric acid was used to figure out the relationship between petroleum HCE and rock dissolution quantity in dissolution emission model. All the experiment methods are shown below.

Corrosion experiment in the field

Before the experiment, all rock samples were prepared into cubes (about $5 \times 5 \times 1 \text{ cm}^3$) (Fig. S4). Three duplicate samples were prepared to get reliable results. All the samples were washed with deionized water and dried for 8 h at 100 °C. Then, they were weighed using an electronic balance (BSA3202S-CW) (Table S5).

To simulate the rock corrosion in natural environment, all the samples were buried 15 cm underground where they were sampled (Fig. S5). The experiment was done for a year, i.e., April 9, 2016, to April 9, 2017. The amount of rainfall during the stated period was about 1436.7 mm.

Corrosion emission model in the laboratory

The ability of water-rock-hydrocarbon interaction relates to the chemical constitutions of groundwater, rock, and reaction environment (Jia et al. 2018). However, there are too many interferences and uncontrollable factors in natural environment. It is hard to determine the contribution and driving force of HCE for each factor. Therefore, in this model, a single factor was used to find out the main factor of water-rock-hydrocarbon interaction.

Basically, pH and salinity of groundwater are the key factors for rock corrosion (Jiang et al. 2000). Based on the

chemical constituents of shallow groundwater in the area, this model used reactant solution with different pH and salinity to figure out the hydrocarbons' migration, respectively.

Even though the stratum has hydrocarbon potential in the area, the release ability is still very low compared with the source rock in oil-gas field. Moreover, the water-rock interaction is a long-term geological process in nature. To promote this process, the relatively high hydrocarbon potential strata in the area were chosen, which were T_{1yn}^{4-1} , T_{1yn}^{4-2} , and T_{2g}^{3-3} . In addition, 100 g of each rock was used in the model. Before the experiment, the diameter of rock samples was reduced to less than 0.15 mm.

The base solution for preparing the reactant solution was deionized water. In the area, pH of all shallow groundwater was 7.89–8.50 (Table S3), indicating that all the samples are alkalescence groundwater. Otherwise, acidic condition may promote the dissolution of carbonate rocks. Eventually, pH for a range of the reactant solution was prepared as 4, 5, 7, 8, and 9. A dilute hydrochloric acid (HCl) was used to adjust the pH = 4 and 5 because a weak HCl does not hydrolyze hydrocarbons. And calcium oxide was used to produce pH = 8 and 9. Deionized water was used to produce pH = 7 (Table S6). A series of salinity solution was prepared in the laboratory as 30 mg/L, 200 mg/L, and 600 mg/L (Table S6), since the observed salinity in all shallow groundwater was 111–630 mg/L (Table S3). In addition, the major constituents in shallow groundwater were Ca^{2+} , Mg^{2+} , SO_4^{2-} , and HCO_3^- . Magnesium sulfate (MgSO_4) was used to adjust the salinity excluding calcium sulfate (CaSO_4) that hardly dissolve in water (Table S6). Duplicate samples were prepared to get reliable results (Table S6).

To simulate the shallow aquifer environment, all the samples (the rock and reactant solution) were stocked under room temperature, pressure, and oxidation conditions and kept in the dark for 4 months. During the experimental period, all the samples had been kept oscillating to promote rock contact with reactant solution (Fig. S6). The volume of reactant solution for samples WR-01–WR-54 was 1 L to determine cation, anion, and petroleum hydrocarbon concentration. Otherwise, the volume of reactant solution for WR-55 to 61 was 5 L to determine biomarkers (Table S6).

Dissolution emission model in the laboratory

The relatively high hydrocarbon potential rock in each stratum was chosen to compare the HCE ability. One hundred grams of each rock was prepared (Table S7). Before the experiment, the diameter of rock samples was reduced to less than 0.15 mm to promote the reactions.

Preparation of the reactant solution used HCl. Based on the major components of stratum in the area (Table S2), the concentration of HCl was prepared as shown in Table S7 to get different dissolution levels.

Rocks and reactant solution were mixed under room temperature and pressure. After the reaction, supernatant liquor was taken to analyze the concentration of hydrocarbon (Fig. S7).

Analysis

For rock samples, X-ray fluorescence spectrometry (XRF-1800, Shimadzu Sequential X-ray Fluorescence Spectrometer) and Rock-Eval Pyrolysis (OGE-II) produced data on the major chemical constituents and total organic carbon (TOC), respectively. In addition, an electronic balance (BSA3202S-CW) determined the weight of rocks. At least three duplicate experiments were done for samples to obtain reliable data. For liquid samples, including shallow groundwater, deep groundwater, and experiment samples, atomic emission spectrometry (iCAP 6300), ion chromatography (ICS1100), titration, infrared spectrophotometry (OIL-8), and GC/MS (Agilent6890N/5795MSD) determined cation, anion, petroleum hydrocarbon concentration, and biomarker characteristics, respectively. The duplicate samples were more than 10%. The standard deviation in duplicate samples was less than 5% with an ion balance deviation of less than 5%, indicating that the results were reliable and consistent.

Hydrocarbon emission estimation

Assumed conditions

Karst aquifers have a complicated groundwater flow regime. To estimate the maximum possible concentration of petroleum hydrocarbon and equal the enrichment to attenuation of groundwater circulation, several assumptions were set. Firstly, the estimating was done in the DLJ system, which is an independent groundwater system. The second assumed that huge karst tunnels did not exist in the system. Thirdly, only water-rock interaction contributed mineral elements to groundwater. The fourth assumption was that the entire hydrocarbon emitted from stratum migrates into groundwater and distributed uniformly. Lastly, groundwater in the DLJ system is mainly from the recharge, which was controlled by the precipitation recharge coefficient and annual average rainfall.

Corrosion equation

According to the previous study, the corrosion rate could be calculated as follows:

$$ER = (W_1 - W_2) \times 10^7 \times 365 / T / S_c \quad (1)$$

where ER is the annual average corrosion rate per unit area ($\text{mg m}^{-2} \text{a}^{-1}$), W_1 is the weight of samples before the experiment (g), W_2 is the weight of samples after the experiment (g), T is

the experimental period (days), and S_c is the superficial area of samples (m^2) (Yuan and Cai 1988).

Groundwater volume estimation in the DLJ system

Additionally, according to the assumptions, the volume of groundwater runoff in the DLJ system could be calculated as follows:

$$V = S_s \times P \times \mu \quad (2)$$

where S_s is the area of different lands using (km^2), P is the annual average rainfall (mm), and μ is the precipitation recharge coefficient of different land use (dimensionless). Based on the statistical data of land use in karst area of southwest China (Yuan 2007) and land use distribution of the area (Fig. S3), the precipitation recharge coefficients of habitation, arable land, woodland, and stony desertification were 0.002, 0.032, 0.275, and 0.346, respectively. The annual average rainfall was about 1402.8 mm. By calculating, the groundwater runoff in the DLJ system was estimated as 1.03×10^{10} L.

Hydrocarbon estimation equation

Based on these five assumptions, the concentration of petroleum hydrocarbon relates to HCE from the stratum and groundwater runoff in the DLJ system. The equation could for the preceding statement present as follows:

$$C = w / V \quad (3)$$

where C is the concentration of petroleum hydrocarbon in the DLJ system (mg L^{-1}), w is the quantity of HCE from stratum (g), and V is the volume of groundwater runoff in the DLJ system (L).

Results and discussion

Corrosion rate for all stratum in natural environment

According to Eq. 1, Table 1 shows the corrosion rate of T_2f , T_2g^3 , T_2g^2 , and T_1yn^4 ranged from 1.13×10^4 to $2.54 \times 10^4 \text{ mg m}^{-2} \text{a}^{-1}$, 1.94×10^4 to $5.11 \times 10^4 \text{ mg m}^{-2} \text{a}^{-1}$, 0.28×10^4 to $1.49 \times 10^4 \text{ mg m}^{-2} \text{a}^{-1}$, and 0.65×10^4 to $1.74 \times 10^4 \text{ mg m}^{-2} \text{a}^{-1}$, respectively. While the corrosion rate of T_2g^1 and T_1yn^3 was $4.68 \times 10^4 \text{ mg m}^{-2} \text{a}^{-1}$ and $0.69 \times 10^4 \text{ mg m}^{-2} \text{a}^{-1}$, respectively, revealing the corrosion rate mainly depended on the lithology of different strata in this experiment. As we know, the corrosion rate in such field experiment is determined by many factors, such as lithology, climate, rainfall, structure of rocks, and hydrogeological condition, indicating it was hard to get a relatively accurate corrosion rate. However, Jiang et al.'s research had done the similar corrosion

Table 1 The results of corrosion experiment in the field

Samples	Stratum	W ₁ (g)	W ₂ (g)	ER (mg m ⁻² a ⁻¹)	Samples	Stratum	W ₁ (g)	W ₂ (g)	ER (mg m ⁻² a ⁻¹)
YY-01-a	T ₂ f ³	69.7440	69.7043	1.13 × 10 ⁴	YY-08-a	T ₂ g ²⁻²	73.6055	73.5961	0.28 × 10 ⁴
YY-01-b		69.3024	69.2624		YY-08-b		74.4760	74.4642	
YY-01-c		71.3333	71.2711		YY-08-c		70.4266	70.4126	
YY-02-a	T ₂ f ²	66.5917	66.4522	2.08 × 10 ⁴	YY-09-a	T ₂ g ²⁻¹	71.8186	71.7548	1.49 × 10 ⁴
YY-02-b		65.0954	65.0227		YY-09-b		70.0952	70.0326	
YY-02-c		66.3969	66.3267		YY-09-c		67.1601	67.1017	
YY-03-a	T ₂ f ⁴	70.2565	70.1929	2.54 × 10 ⁴	YY-10-a	T ₂ g ¹	60.6345	60.4474	4.68 × 10 ⁴
YY-03-b		71.8266	71.7757		YY-10-b		61.3220	61.1269	
YY-03-c		71.3236	71.1197		YY-10-c		65.2772	65.0834	
YY-04-a	T ₂ g ³⁻³	71.5267	71.4246	2.88 × 10 ⁴	YY-11-a	T ₁ yn ⁴⁻²	62.8690	62.8152	1.74 × 10 ⁴
YY-04-b		72.0139	71.9052		YY-11-b		71.7737	71.6996	
YY-04-c		70.1675	70.0538		YY-11-c		73.2878	73.2241	
YY-05-a	T ₂ g ³⁻²	64.4161	64.0670	5.11 × 10 ⁴	YY-12-a	T ₁ yn ⁴⁻¹	72.2242	72.1993	0.65 × 10 ⁴
YY-05-b		67.9657	67.8711		YY-12-b		69.3953	69.3715	
YY-05-c		66.1926	66.1474		YY-12-c		71.2932	71.2621	
YY-06-a	T ₂ g ³⁻¹	68.2982	68.2113	1.94 × 10 ⁴	YY-13-a	T ₁ yn ³	71.6356	71.6044	0.69 × 10 ⁴
YY-06-b		76.3571	76.2764		YY-13-b		74.1216	74.0906	
YY-06-c		73.3386	73.2892		YY-13-c		75.4401	75.4162	
YY-07-a	T ₂ g ²⁻³	68.5025	68.4841	0.77 × 10 ⁴	Rainfall was about 1436.7 mm since April 9, 2016, to April 9, 2017				
YY-07-b		73.4936	73.4682						
YY-07-c		68.5439	68.5200						

rate test for T₂g³⁻² in Guiyang (150 km away from the research area, with average annual rainfall about 1400 mm and the carbonate rock lithology) in 2000. They observed the corrosion rate of T₂g³⁻² was about 1.68 × 10⁴ mg m⁻² a⁻¹ (Jiang et al. 2000). Comparing with Jiang et al.'s research, the corrosion rate of T₂g³⁻² in the present research (5.11 × 10⁴ mg m⁻² a⁻¹) had the same order of magnitude, indicating the results from the corrosion experiment in the field were reliable.

Relation between petroleum hydrocarbon emission and rock corrosion in the laboratory

The water-rock interaction is a tedious process. To figure out the magnitude of HCE from stratum and to save the time-cost, samples with the most HCE potential were tested in preliminary analysis.

The degree of water-rock interaction

Table 2 shows the hydrocarbon could barely be detected in the 4-month period, indicating the degree of water-rock-hydrocarbon was relatively low in this experiment. The corrosion quality ranged from 0.08 to 1.92 g. Comparing with the mineral constituent of reactant solution before the experiment, the mineral constituent of reactant solution was totally changed in 4 months, such as the concentration of Ca²⁺, K⁺ Mg²⁺, Na⁺, Cl⁻, NO₃⁻, and SO₄²⁻ had increased in all the

analyzed samples (Table 2). Moreover, the concentrations of Ca²⁺ from WR-16 and WR-35 were 97.7 mg L⁻¹ and 46.4 mg L⁻¹, respectively, which were much higher than other samples (Table 2), indicating the high-salinity reactant solution increased calcium dissolution, demonstrating the relatively strong water-rock interaction, while the mineral constituent of WR-19, 21, 23, 25, and 27 were similar, such as concentration of Ca²⁺, K⁺ Mg²⁺, Na⁺, Cl⁻, NO₃⁻, and SO₄²⁻ ranged from 10.6 to 17.5 mg L⁻¹, 2.59 to 2.89 mg L⁻¹, 9.03 to 12.7 mg L⁻¹, 3.11 to 4.48 mg L⁻¹, 7.18 to 7.69 mg L⁻¹, 0.704 to 1.77 mg L⁻¹ and 10.1 to 11.7 mg L⁻¹, respectively, revealing different pH values had less effect on T₁yn⁴⁻² corrosion.

Biomarker characteristics

Biomarker characteristics showed that hydrocarbons migrated from rocks to reactant solution (Liu et al. 2017). The results of Fig. 3 and Table 3 showed the hydrocarbon migration from rock to reactant solution actually happened during the experiment period. For T₂g³⁻³, the distribution of saturated hydrocarbon lying between nC16 and nC36 in WR-60 and WR-61 was similar to that in SK-01, SK-04, SK-05, and SK-07. Moreover, the distribution of saturated hydrocarbon lying between nC25 and nC30 in WR-60 and WR-61 was similar to that in YY-04. For T₁g⁴⁻², the distribution of saturated hydrocarbon lying between nC24 and nC32 in WR-58 and WR-59 was similar to that in YY-11. For T₁g⁴⁻¹, the distribution of

Table 2 Results of mineral constituent, corrosion, and hydrocarbons emission after 4 months

Samples	Stratum	Initial condition		Results										
		pH	Salinity (mg L ⁻¹)	Ca ²⁺ (mg L ⁻¹)	K ⁺ (mg L ⁻¹)	Mg ²⁺ (mg L ⁻¹)	Na ⁺ (mg L ⁻¹)	Cl ⁻ (mg L ⁻¹)	NO ₃ ⁻ (mg L ⁻¹)	SO ₄ ²⁻ (mg L ⁻¹)	pH	Petroleum hydrocarbon (mg L ⁻¹)	Corrosion quality (g)	
WR-01	YY-12 (T ₁ yn ⁴⁻¹)	4.00	-	29.2	2.16	10.8	1.14	5.41	1.03	48.4	8.04	0.02	1.02	
WR-02				30.3	2.18	11.2	1.11	5.19	0.756	49.9	8.19	ND	1.03	
WR-16			600	97.7	2.86	83.2	1.66	5.10	0.713	676	8.05	ND	1.06	
WR-19	YY-11 (T ₁ yn ⁴⁻²)	4.00	-	17.5	2.65	12.7	3.14	7.18	0.704	10.1	8.34	ND	0.42	
WR-21		5.00		14.6	2.59	10.9	3.11	7.43	1.77	10.2	8.47	ND	0.32	
WR-23		7.00		16.0	2.80	11.9	3.19	7.69	1.70	11.7	8.44	ND	0.29	
WR-25		8.00		11.2	2.89	9.35	3.83	7.57	0.857	10.4	8.68	ND	0.31	
WR-27		9.00		10.6	2.79	9.03	4.48	7.42	1.01	10.3	8.72	ND	0.56	
WR-30		-	30	15.6	2.81	13.3	3.71	7.46	1.02	30.3	8.23	ND	0.11	
WR-32			200	32.0	2.77	35.7	3.46	7.51	0.946	164	8.26	ND	0.12	
WR-35			600	46.4	2.89	82.3	3.37	7.28	0.537	498	8.36	ND	0.09	
WR-39	YY-04 (T ₂ g ³⁻³)	5.00	-	13.3	0.24	2.91	0.69	4.94	1.08	13.0	8.40	ND	0.59	
WR-48		-	30	16.2	0.29	5.48	0.90	5.24	0.858	32.7	8.72	ND	0.22	

ND not detected

saturated hydrocarbon lying between nC26 and nC30 in WR-55, WR-56, and WR-57 was similar to that in YY-12, showing the distribution range of saturated hydrocarbon in rock, groundwater, and reactant solution was similar from the same stratum. Additionally, the odd-even predominance (OEP), carbon preference index (CPI), and pristane/phytane value were similar between reactant solution and deep groundwater (Table 3). These results determined the hydrocarbons in rocks, deep groundwater, and reactant solution sharing the same origin. Since the hydrocarbons in T₂g³ and T₁yn⁴ were derived from lower aquatic with terrigenous detrital organic matter contribution deposited under marine conditions, the main peak of saturated hydrocarbon in rocks was identified as nC16 and nC18, respectively, which belonged to light saturated hydrocarbon (Fig. 3), while, after the migration, the main peak of saturated hydrocarbon in groundwater and reactant solution changed to nC25, nC26, and nC27 (Fig. 3) which belonged to heavy saturated hydrocarbon. The physicochemical property of hydrocarbons might be the main reason for these biomarker succession and mutation. As we know, the octanol-water partition coefficient increases with carbon numbers (Mackay 2006). Moreover, light saturated hydrocarbon with low octanol-water partition coefficient was easy to vaporize, while heavy saturated hydrocarbon with high octanol-water partition coefficient might remain in water (Mackay 2006; Voutsas 2007) (Table S8). Additionally, groundwater exists in relatively opened and oxidizing environment, while rocks exist in relatively enclosed and reducing environment. The difference of existence conditions may impel the light saturated hydrocarbons to transfer to air from groundwater.

Maximum hydrocarbon emission ability in rock dissolution experiment in the laboratory

Hydrocarbon emission ability

Table 4 shows the maximum HCE concentration of T₁yn⁴ and T₂g³ was 0.10 mg L⁻¹ and 0.09 mg L⁻¹, respectively, which was much higher than that of other strata. Moreover, high rock dissolution quality led to relatively high concentration of hydrocarbon in T₁yn⁴ and T₂g³. However, in T₁yn³, T₂g¹, T₂g², and T₂f, the rock dissolution rate and concentration of petroleum hydrocarbon did not show a linear relation, indicating the HCE ability for relatively low-level hydrocarbon potential stratum was limited.

Hydrocarbon emission process

Although rocks dissolution led to the relatively high concentration of petroleum hydrocarbon, the HCE process was very different for T₁yn⁴ and T₂g³. In Fig. 4, the HCE process of T₁yn⁴ shows a sharp changing beyond 75 g. The concentration of petroleum HCE was stable around 0.03 mg/L prior to the

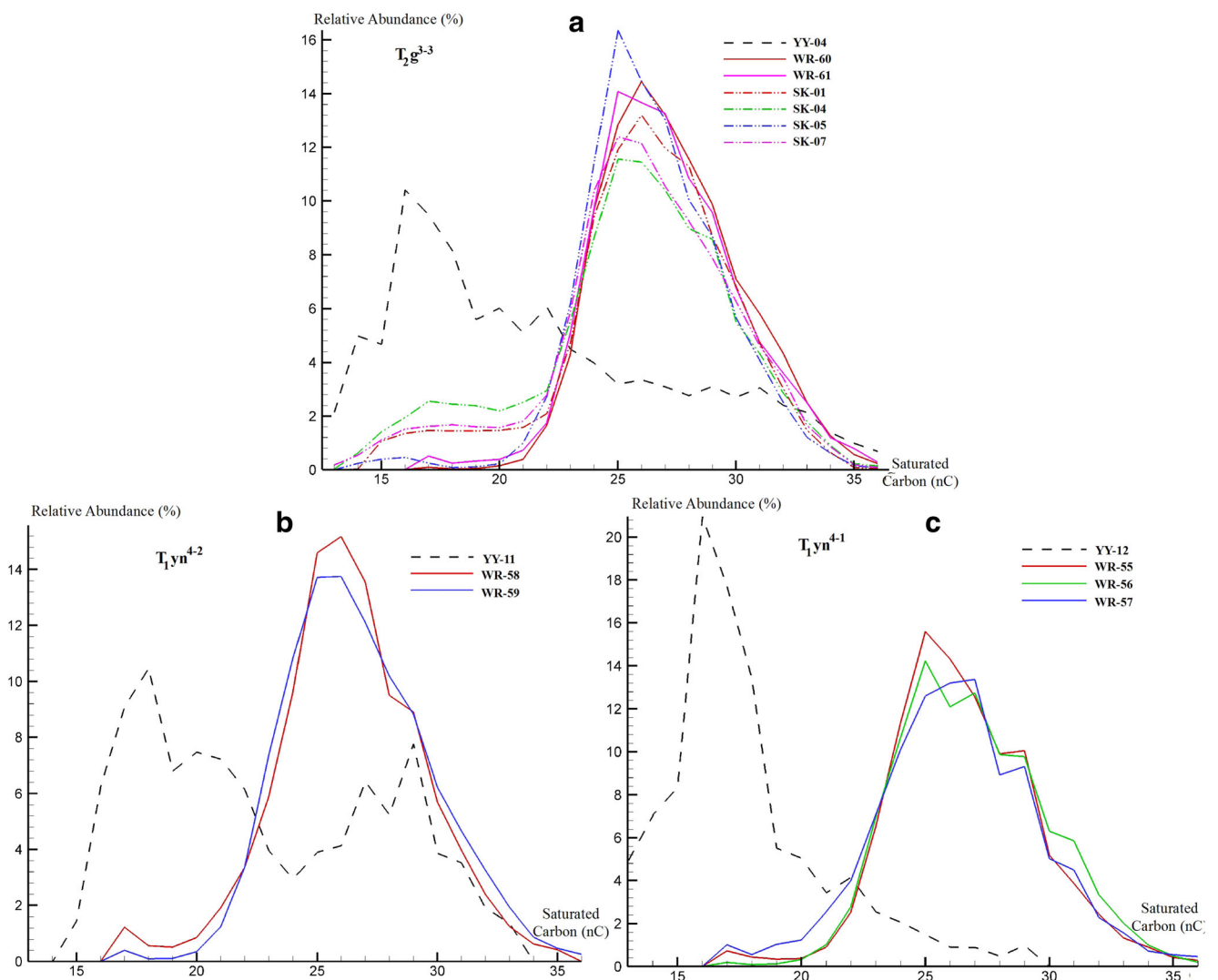


Fig. 3 Relative abundance of saturated carbon of experiment samples, rocks, and deep groundwater. Solid line shows the relative abundance of saturated carbon of experimental samples. Dashed line shows the relative abundance of saturated carbon of rocks. Dashed with dot line shows the relative abundance of saturated carbon of deep groundwater. **A** shows the

relative abundance of saturated carbon of experiment samples, rocks, and deep groundwater from T₂g³⁻³. **B** shows the relative abundance of saturated carbon of experiment samples and rocks from T₁yn⁴⁻². **C** shows the relative abundance of saturated carbon of experiment samples and rocks from T₂g⁴⁻¹

rate of 75 g. Between 75 and 85 g, the concentration of petroleum HCE increased sharply to 0.10 mg L⁻¹. Otherwise, for T₂g³, the concentration of petroleum HCE increased gradually to 0.09 mg L⁻¹, revealing hydrocarbons distributed more uniformly in T₂g³ than those in T₁yn⁴. Additionally, during the process of oil generation, the hydrocarbons in hydrocarbon reservoir stratum might migrate from other hydrocarbon source strata through fracture and enriched in some parts of hydrocarbon reservoir stratum, which might lead hydrocarbons to distribute more uniformly in hydrocarbon source stratum than that in hydrocarbon reservoir stratum (Onojake et al. 2015), indicating, T₂g³ would be more likely to be the hydrocarbon source stratum in the study area, while T₁yn⁴ would be more likely to be the hydrocarbon reservoir stratum.

Distribution characteristics of high hydrocarbon groundwater in the DLJ system

Table S3 shows the concentration of petroleum hydrocarbon in the DLJ system ranged from not detected to 0.14 mg L⁻¹. Figure 5 reveals water-rock-hydrocarbon interaction and groundwater circulation would influence the concentration of petroleum hydrocarbon. The enrichment and attenuation of groundwater circulation controls the distribution of petroleum hydrocarbon. In the 2nd lateral recharge zone, the petroleum hydrocarbon concentration of SY-09, SY-06, and SY-05 was not detected, 0.04 mg L⁻¹ and 0.12 mg L⁻¹, respectively, showing the concentration of petroleum hydrocarbon mainly increased

Table 3 Biomarker parameters of rock, deep groundwater, and experimental samples

Samples		Stratum	N-alkanes					Isoprenoid
			Range	Main peak	OEP	CPI	Pr/Ph	
YY-04	Rocks	T ₂ g ³⁻³	nC13~nC36	16	0.84	1.06	1.63	
SK-01	Deep groundwater		nC13~nC36	26	1.10	1.00	1.29	
SK-04			nC13~nC36	25	1.12	1.11	1.48	
SK-05			nC14~nC36	25	1.04	1.14	0.92	
SK-07			nC13~nC36	25	1.05	1.03	1.66	
WR-60	Experimental samples	nC17~nC36	26	1.03	1.04	1.54		
WR-61		nC17~nC36	25	1.06	1.11	1.56		
YY-11	Rocks	T ₁ yn ⁴⁻²	nC15~nC33	18	0.79	1.40	1.26	
WR-58	Experimental samples		nC17~nC36	26	1.10	1.13	1.42	
WR-59		nC17~nC36	26	1.28	1.07	1.46		
YY-12	Rocks	T ₁ yn ⁴⁻¹	nC13~nC29	16	0.78	1.69	1.95	
WR-55	Experimental samples		nC17~nC36	25	1.13	1.16	1.34	
WR-56			nC17~nC36	25	1.18	1.21	1.42	
WR-57			nC17~nC36	27	1.37	1.21	1.41	

OEP odd-even predominance, CPI carbon preference index, Pr/Ph pristane/phytane ratios

with the runoff, indicating water-rock interaction would lead to HCE. Moreover, the concentration of petroleum hydrocarbon in the lateral recharge zone is higher than that in the main runoff zone, indicating the groundwater circulation may be diluting the concentration of petroleum hydrocarbon. However, in the discharge zone, the petroleum hydrocarbon concentration of SY-08 and SY-10 were 0.08 mg L⁻¹ and 0.14 mg L⁻¹, respectively, higher than most samples, indicating the interaction would enrich the petroleum hydrocarbon and increase the concentrations in the area, where the hydrodynamic condition was not satisfactory.

Hydrocarbon estimation

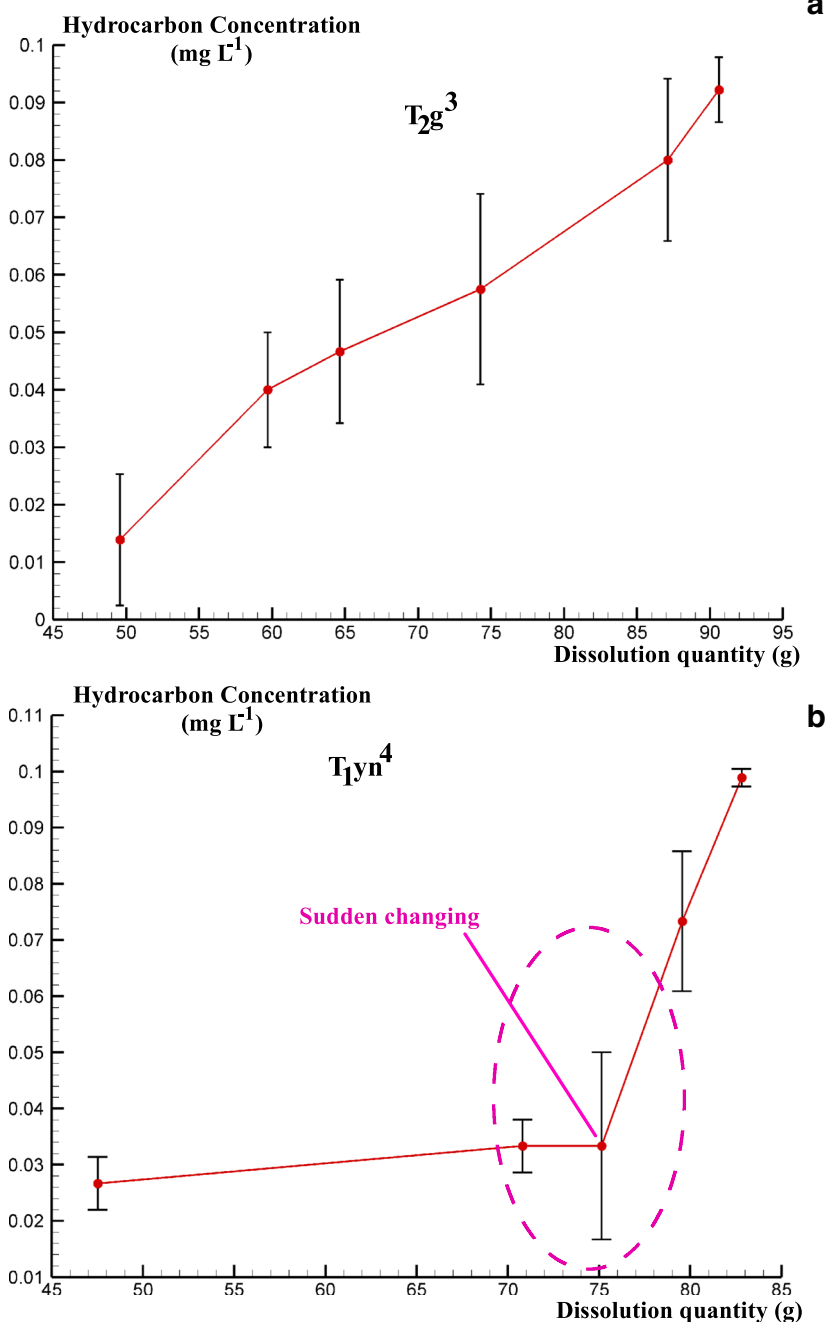
According to assumed conditions, local hydrogeological condition, land use types, and Eq. 3, the quantity of HCE from stratum would determine the hydrocarbon concentration of groundwater in the DLJ system. Additionally, based on the results of experiments above, hydrocarbon concentration of groundwater was related to the corrosion quantity of relatively high hydrocarbon potential strata, which were T₁yn⁴ and T₂g³ in the study. Normally, the corrosion quantity of stratum could be estimated according to corrosion rates (Jiang et al. 2000), which were the results of corrosion

Table 4 Results of dissolution and hydrocarbons emission

Samples	Stratum	C _{HCl} (mol L ⁻¹)	Petroleum hydrocarbon (mg L ⁻¹)	Dissolution quality (g)	Samples	Stratum	C _{HCl} (mol L ⁻¹)	Petroleum hydrocarbon (mg L ⁻¹)	Dissolution quality (g)
RD-01	YY-13	2.0	0.02	90.18	RD-12	YY-07	2.1	0.04	96.12
RD-02	(T ₁ yn ³)	1.5	0.02	71.20	RD-13	(T ₂ g ²⁻³)	1.8	0.04	85.34
RD-03		1.0	0.02	48.05	RD-14		1.0	0.03	49.07
RD-04	YY-11	2.0	0.10	82.82	RD-15	YY-04	2.0	0.09	90.62
RD-05	(T ₁ yn ⁴⁻²)	1.7	0.07	79.56	RD-16	(T ₂ g ³⁻³)	1.8	0.08	87.10
RD-06		1.6	0.03	75.15	RD-17		1.5	0.06	74.29
RD-07		1.5	0.03	70.81	RD-18		1.3	0.05	64.63
RD-08		1.0	0.03	47.52	RD-19		1.20	0.04	59.70
RD-09	YY-10	1.2	0.05	40.04	RD-20		1.0	0.01	49.58
RD-10	(T ₂ g ¹)	0.60	0.05	27.25	RD-21	YY-02	2.1	0.02	98.95
RD-11		0.30	0.05	14.04	RD-22	(T ₂ f ²)	1.8	0.02	88.44
					RD-23		1.0	0.02	48.95

The concentration of petroleum hydrocarbons and the dissolution rate of rocks were mean value from multi-experiments

Fig. 4 The hydrocarbon emission process. **A** shows the hydrocarbon emission process of T_2g^3 . **B** shows the hydrocarbon emission process of T_1yn^4



experiment in the field. Besides that, in the 4-month corrosion emission model in the laboratory, the mineral constituent of groundwater had totally changed when the corrosion quality increased, especially for Ca^{2+} and Mg^{2+} , indicating mineral constituent of groundwater might reflect the degree of rock corrosion in the local. Therefore, both corrosion rate of rocks and concentration of Ca^{2+} and Mg^{2+} could be used to estimate hydrocarbon concentration of groundwater in the area, which were named as “corrosion rate estimation method” and “mineral constituent estimation method” in this research.

Corrosion rate estimation method of hydrocarbon

The estimation method was based on the results of corrosion experiment done in the field and dissolution emission model. Making the necessary substitutions using Eqs. 1 and 2 results in expansion of Eq. 3 as:

$$C = (S_A \times H_A \times ER \times S_c \times a/100/V_c)/(S_s \times P \times \mu) \quad (4)$$

where a is the HCE from per 100-g rocks (mg), which is 0.09 mg and 0.1 mg for T_2g^3 and T_1yn^4 , respectively. S_A is

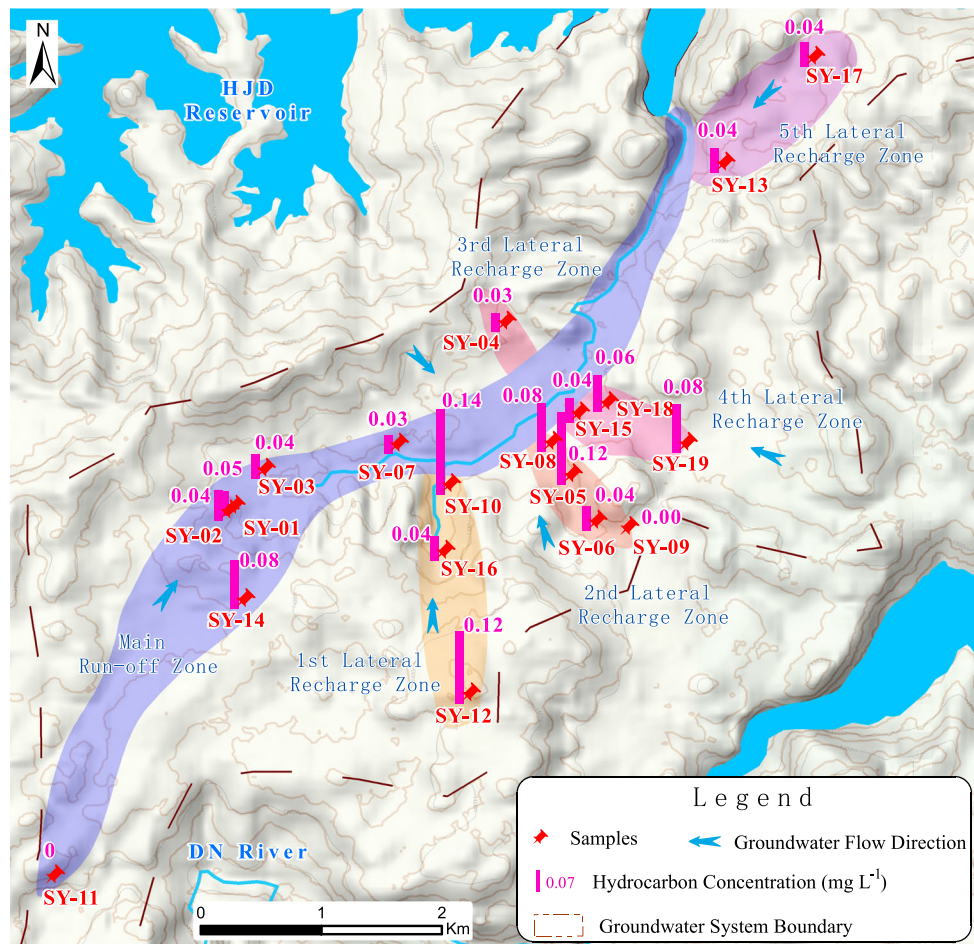


Fig. 5 Spatial distribution of hydrocarbon in the DLJ system

the area of hydrocarbon generation stratum (km^2), which is 12.6 km^2 and 0.69 km^2 for $T_2 g^3$ and $T_1 yn^4$, respectively. H_A is the average thickness of hydrocarbon generation stratum (m), which is 257 m and 89.5 m for $T_2 g^3$ and $T_1 yn^4$, respectively. ER is the annual average corrosion rate per unit area ($\text{mg m}^{-2} \text{ a}^{-1}$), which is $2.88 \times 10^4 \text{ mg m}^{-2} \text{ a}^{-1}$ and $1.74 \times 10^4 \text{ mg m}^{-2} \text{ a}^{-1}$ for $T_2 g^3$ and $T_1 yn^4$, respectively. S_c is the specific surface area of corrosion experiment samples (m^2), which is $7.11 \times 10^{-3} \text{ m}^2$ and $6.93 \times 10^{-3} \text{ m}^2$ for $T_2 g^3$ and $T_1 yn^4$, respectively. V_c is the volume of corrosion experiment samples (m^3), which is $2.50 \times 10^{-5} \text{ m}^3$ for both $T_2 g^3$ and $T_1 yn^4$. The other variables are as explained in Eqs. 1, 2, and 3. Based on the hydrogeology setting and experimental data, the annual average concentration of petroleum hydrocarbon in the DLJ system was calculated as 2.35 mg L^{-1} .

Mineral constituent estimation method of hydrocarbon

As stated earlier, calcite and dolomite are the main constituents of stratum in karst aquifers. In the area, the lithology of $T_2 g^3$ and $T_1 yn^4$ was mainly calcite-dolomite, which

would release Ca^{2+} and Mg^{2+} into groundwater by water-rock interaction. Based on chemical equation of calcite-dolomite corrosion, pure dolomite would release equal concentration of Ca^{2+} and Mg^{2+} . However, calcite-dolomite corrosion would vary the concentration ratio of Ca^{2+} to Mg^{2+} . The estimation used individual concentrations of Ca^{2+} and Mg^{2+} to calculate the maximum and minimum corrosion quality of rocks, respectively. Additionally, based on the assumptions, the groundwater in the main runoff-discharge zone was considered to have reached solubility equilibrium, such as SY-08 and SK-07 (Fig. 2). Moreover, all the mineral elements in these samples were from water-rock interaction. Therefore, the concentration of Ca^{2+} and Mg^{2+} of SY-08 and SK-07 was selected to estimate the maximum and minimum corrosion quality of rocks, respectively. According to the equations mentioned before, the hydrocarbon concentration could be estimated as follows:

$$C = (M_m \times a_{\text{average}}/100)/V \tag{5}$$

where M_m is the corrosion quality (mg). $a_{average}$ is the average of HCE from per 100-g T_2g^3 and T_1yn^4 , which is 0.095 mg. Moreover, the M_m could be calculated as follows:

$$M_m = C_m \times V \tag{6}$$

where C_m is the corrosion quality from per liter groundwater ($mg\ L^{-1}$). Additionally, the main component of calcite-dolomite is $CaMg(CO_3)_2$. According to the chemical equation of calcite-dolomite corrosion, 1 mol $CaMg(CO_3)_2$ would release 1 mol Ca^{2+} and 1 mol Mg^{2+} , respectively. Eventually, the concentration range of hydrocarbon in the DLJ system was estimated from 0.05 to 0.50 $mg\ L^{-1}$ (Table 5).

Comparison of the different estimation methods

The concentration of hydrocarbon estimated by corrosion rate estimation method was 2.35 $mg\ L^{-1}$, which was ten times greater than the maximum result of groundwater samples in the area (Table S3). This could be concluded from two perspectives. Firstly, the volume of stratum could hardly be calculated because of the complexity of figuring out the spatial structure of the stratum. Then, the corrosion rate could not simply accumulate by the results of corrosion experiment, which would enlarge the corrosion rate. Otherwise, if the corrosion due to fissure and corrosion experiment samples had developed representational fissure, this method could get the relatively exact corrosion rate and concentration of hydrocarbon.

The concentration of hydrocarbon estimated by mineral constituent estimation method ranged from 0.05 to 0.50 $mg\ L^{-1}$, which was consistent with the results of groundwater samples in the study area (Table S3). Additionally, by using this method, the concentration of petroleum hydrocarbon was related to the concentration of Ca^{2+} and Mg^{2+} , which determined water-rock interaction that would lead to the HCE. This method was close to reality. Otherwise, enrichment, attenuation of groundwater circulation, and supersaturated precipitation of Ca^{2+} and Mg^{2+} might also influence the result of the estimation. Hydrogeology and geological setting of the study area should be analyzed emphatically when using this method.

Conclusions

This research focused on the factors and processes involved in hydrocarbon migration from stratum to shallow Triassic aquifer of northwestern Guizhou, China. By designing the corrosion emission and dissolution emission models in the laboratory, salinity might be considered the main driving

Table 5 Results of hydrocarbon groundwater estimation by mineral constitution estimation method

Samples	Estimation based on the concentration of Ca^{2+}				Estimation based on the concentration of Mg^{2+}				V (L)	$a_{average}$ (mg)	
	Ca^{2+} ($mg\ L^{-1}$)	Corrosion concentration ($mg\ L^{-1}$)	Corrosion quality (mg)	Hydrocarbon quality (mg)	Mg^{2+} ($mg\ L^{-1}$)	Corrosion concentration ($mg\ L^{-1}$)	Corrosion quality (mg)	Hydrocarbon quality (mg)			C ($mg\ L^{-1}$)
SY-08	27.0	124	1.3×10^{12}	1.2×10^9	6.68	51.2	5.3×10^{11}	5.0×10^9	0.05	1.03×10^{10}	0.095
SK-07	115	530	5.4×10^{12}	5.2×10^9	30.6	235	2.4×10^{12}	2.3×10^9	0.22		

force for water-rock-hydrocarbon interaction in the study area. Relatively high salinity promotes the rock corrosion and increases the concentration of mineral constituent in groundwater. Moreover, in relatively high hydrocarbon potential strata, the HCE increased with rock dissolution. The maximum HCE of $T_1y_n^4$ and T_2g^3 was 0.10 mg L^{-1} and 0.09 mg L^{-1} , respectively. However, the HCE process was influenced by hydrocarbon distribution in the stratum suggesting that T_2g^3 would be the hydrocarbon source stratum in the area. Comparing different HCE estimation method, the results estimated by mineral constituent estimation method was similar to the hydrocarbon concentration of groundwater in the area, indicating the original hydrocarbon concentration related to the concentration of Ca^{2+} and Mg^{2+} in shallow groundwater in karst area. This research just presented a method that hydrocarbon concentration of groundwater could be estimated in karst area. Many environmental conditions were set as ideal conditions. An extended period of study, inclusion of more reactions, and analysis of various factors are still needed in the future to finding out the HCE process in relatively low degree of water-rock-hydrocarbon interaction. Coupled to this, verifying the results with field data is recommended in future studies. Also, verification of estimation of high hydrocarbon groundwater should be done in the research area to figure out the applicability of this method.

Acknowledgments The authors honorably appreciate the China Hydrogen and Oxygen Environment Testing Co. Ltd for technical support during sample testing. Furthermore, Dr. Jin Xiaowen and Miss Li Yanni deserve special mention for their contribution in the discussion of this work.

Funding information This research was financially supported by the groundwater environmental impact assessment project for the annual 600,000 tons polyolefin production chemical plant in Zhijian, Guizhou, China.

References

- Adekunle AS, Oyekunle J, Ojo OS, Maxakato NW, Olutona GO, Obisesan OR (2017) Determination of polycyclic aromatic hydrocarbon levels of groundwater in Ife north local government area of Osun State, Nigeria. *Toxicol Rep* 4:39–48
- Anatolievich DN, Mikhailovich SM (2017) Hydrogeochemistry of the Arctic areas of Siberian petroleum basins. *Pet Explor Dev* 44(5): 780–788
- Belousova AP, Krainov SR, Ryzenko BN (1998) Evolution of groundwater chemical composition under human activity in an oilfield. *Environ Geol* 38:34–46
- Bonzani I, Monaco R, Zavattaro MG (2016) Understanding shallow and deep flow to assess the risk of hydrocarbon development on groundwater quality. *Mar Pet Geol* 78(3):728–737
- Bouchaou L, Warner NR, Tagma T, Hssaisoune M, Vengosh A (2017) The origin of geothermal waters in Morocco: multiple isotope tracers for delineating sources of water-rock interactions. *Appl Geochem* 84:244–253
- Cai CF, Mei BW, Li W, Fan G (1997) Water-rock interaction in Tarim Basin: constraints from oilfield water geochemistry. *Chin J Geochem* 16:289–303
- Chalmers GRL, Bustin RM (2017) A multidisciplinary approach in determining the maceral (kerogen type) and mineralogical composition of Upper Cretaceous Eagle Ford Formation: impact on pore development and pore size distribution. *Int J Coal Geol* 171:93–110
- Collins AG (1974) Geochemistry of oilfield water applied to exploration. *Oil Gas J* 72:21
- Huang SY, Li MJ, Zhang K, Wang TG, Xiao ZY, Fang RH, Zhang BS, Wang DW, Zhao Q, Yang FL (2016) Distribution and geochemical significance of phenylphenanthrenes and their isomers in selected oils and rock extracts from the Tarim Basin, NW China. *Pet Sci* 13: 183–191
- Huang T, Li Y, Pang Z, Wang Y, Yang S (2017) Groundwater baseline water quality in a shale gas exploration site and fracturing fluid-shale rock interaction. *Procedia Earth Planet Sci* 17:638–641
- Jia Y, Fei L, Huang X, Li J, Zhai G (2018) Coupling optimization model embedded groundwater dynamic model for distribution of pumping wells in well irrigation area. *Trans Chin Soc Agric Eng* 34(7):100–106
- Jiang, Z. C., Jiang, X. Z., Lei, M. T. (2000). Estimation of atmospheric CO_2 sink of karst areas in China based on GIS and limestone tablet loss data. *Carsologica Sinica* 19(3):212–217. (Chinese Journal). <https://kns.cnki.net/KCMS/detail/detail.aspx?dbcode=CJFQ&dbname=CJFD2000&filename=ZGYR200003002&v=MDY4NTk4ZVgxTHV4WVM3RGgxVDNxVHJXTTFGcKNUkxPZVorzHFGeUhsVUx6S1B5cINmTEc0SHRITXJJOZab11=>
- Kassotis CD, Vu DC, Vo PH, Lin CH, Cornelius-Green JN, Patton S, Nagel SC (2018) Endocrine-disrupting activities and organic contaminants associated with oil and gas operations in Wyoming groundwater. *Arch Environ Contam Toxicol* 75(2):274–258
- Kerimov VY, Rachinsky MZ, Mustaev RN, Osipov AV (2017) Groundwater dynamics forecasting criteria of oil and gas occurrences in alpine mobile belt basins. *Dokl Earth Sci* 476(1):1066–1068
- Kharaka YK, Law LM, Carothers WW, Goerlitz DF (1986) Role of organic species dissolved in formation water from sedimentary basins in mineral diagenesis. In Gautier DL. Role of Organic Matter in Sediment Diagenesis. *Soc Econ Paleontol Mineral* 38:111–122
- Lasaga AC (1984) Chemical kinetics of water-rock interactions. *J Geophys Res Solid Earth* 89(B6):4009–4025
- Liu S, Qi S, Luo Z, Liu F, Ding Y, Huang H, Chen Z, Cheng S (2017) The origin of high hydrocarbon groundwater in shallow Triassic aquifer in Northwest Guizhou, China. *Environ Geochem Health* 40(1):1–19
- Logeshwaran P, Megharaj M, Chadalavada S, Bowman M, Naidu R (2018) Petroleum hydrocarbons (PH) in groundwater aquifers: an overview of environmental fate, toxicity, microbial degradation and risk-based remediation approaches. *Environ Technol Innov* 10:175–193
- Mackay D (2006) Handbook of physical-chemical properties and environmental fate for organic chemicals. Taylor & Francis, Abingdon
- Onojake MC, Osuji LC, Abrakasa S (2015) Source, depositional environment and maturity levels of some crude oils in southwest Niger Delta, Nigeria. *Chin J Geochem* 34(2):224–232
- Phan TT, Paukert Vankeuren AN, Alexandra Hakala J (2018) Role of water-rock interaction in the geochemical evolution of Marcellus Shale produced waters. *Int J Coal Geol* 191:95–111
- Poi G, Shahsavari E, Aburtomedina A, Mok PC, Ball AS (2018) Large scale treatment of total petroleum-hydrocarbon contaminated

- groundwater using bioaugmentation. *J Environ Manag* 214:157–163
- Ryzhenko BN, Sidkina ES, Cherkasova EV (2015) Thermodynamic modeling of water-rock systems to evaluate their generative potential for hydrocarbons. *Geochem Int* 53(9):825–837
- Sadykova YV, Dul'tseva MG (2017) The role of paleohydrochemical factors in groundwater chemistry formation in oil-and-gas-bearing deposits of the northeastern Bol'shekhetskaya Megasyneclise. *Water Res* 44(2):246–258
- Tissot BP, Welte DH (1984) Petroleum formation and occurrence. Springer Verlag, New York, p 699
- Tissot BP, Durand B, Espitalie J, Combaz A (1974) Influence of nature and diagenesis of organic matter in the formation of petroleum. *AAPG Bull* 58(3):499–506
- Ugochukwu UC, Ochonogor A (2018) Groundwater contamination by polycyclic aromatic hydrocarbon due to diesel spill from a telecom base station in a nigerian city: assessment of human health risk exposure. *Environ Monit Assess* 190(4):249
- Voutsas E (2007) Estimation of the volatilization of organic chemicals from soil. In *Thermodynamics, Solubility and Environmental Issues*. Elsevier Science & Technology Books, Amsterdam, pp 205–227
- Wang F, Cao P, Cao RH, Xiong XG, Hao J (2018) The influence of temperature and time on water-rock interactions based on the morphology of rock joint surfaces. *Bull Eng Geol Environ* 78(5):1–10
- Yasaman R, Yoram E, Reza MH, Mohamad HMG, Asadollah M (2016) Using inverse modeling and hierarchical cluster analysis for hydrochemical characterization of springs and Talkhab River in Tang-Bijar oilfield, Iran. *Arab J Geosci* 9:241
- Yu H, Wang Z, Rezaee R, Zhang Y, Han T, Arif M, Johnson L (2018) Porosity estimation in kerogen-bearing shale gas reservoirs. *J Nat Gas Sci Eng* 52:575–581
- Yuan B H (2007) Research on groundwater resource and environmental geology in the karst mountains area of Southwestern in China. University of Electronic Science and Technology, Chengdu
- Yuan DX, Cai GH (1988) The science of karst environment. Chongqing Publishing Group, Chongqing

Publisher's note Springer Nature remains neutral with regard to jurisdictional claims in published maps and institutional affiliations.